Supplementary Information (SI) for Inorganic Chemistry Frontiers.
This journal is © the Partner Organisations 2025

S/V Co-Doped Ni_2P Microflowers Enable Efficient and Stable Saline Water Electrolysis through Local Microenvironment Engineering

Jiahui Jiang,[a] Yixuan Li,[a] Guancheng Xu,[a,*] Bingbing Gong,[b] Weiwei Wang,[c] Hao Jiang,[b,*] Li Zhang[b,*]

a. State Key Laboratory of Chemistry and Utilization of Carbon Based Energy Resources; College of Chemistry, Xinjiang University, Urumqi, 830017, Xinjiang, PR China.

b. College of Chemical Engineering, Xinjiang University, Urumqi, 830017, Xinjiang, PR China.

c. School of Materials Science and Engineering Xinjiang University, Urumqi, Xinjiang, 830046 China.

* Corresponding author

E-mail: zhangli420@xju.edu.cn, jianghao@xju.edu.cn, xuguancheng@xju.edu.cn,

Material characterization

Phase compositions of the as-made materials were taken on D 8 advance (Germany Bruker) X-ray diffractometer (XRD) with Cu Kα radiation (λ=0.15405 nm). Morphologies of the samples were obtained on a field-emission scanning electronic microscopy (FE-SEM, Hitachi S-4800 microscope) and a high-resolution transmission electronic microscopy (HR-TEM, Hitachi H600 microscope) at an acceleration voltage of 200 kV. At the same time, the elemental content and distribution of the compounds were analyzed by X-ray energy dispersive spectroscopy (EDX) and elemental mapping (HR-TEM, Hitachi H600 microscope). Transmission electron microscopy (TEM) were performed on a Hitachi H600 microscope. X-ray photoelectron spectroscopy (XPS) measurements were performed on a Thermo Fisher Scientific Escalab 250 Xi system operated at 15 kW with a monochromatic Al Kα source, and a base pressure less than 1×10 Mpa under ultra-high vacuum (UHV) and no dust conditions (pass energy = 50.0 eV, dwell time = 136 s, number of scan = 1,

spot size = 500 μm). Raman spectra were obtained on a confocal microscope-based Raman spectrometer (HR Evlution, incident power of 0.15 mW, laser wavelength of 532 nm).

Electrochemical measurements

All electrochemical measurements were tested on CHI-760E electrochemical workstation wich a standard three-electrode system. The obtained materials (1 cm×0.5 cm), Hg/HgO and Graphite rod electrode were used as the working electrode, reference electrode and counter electrode, respectively. All electrochemical tests, including linear sweep voltammograms (LSV), cyclic voltammetry (CV) and electrochemical impedance spectroscopy (EIS) were performed in an 1.0 M KOH aqueous solution at room temperature. All measured potentials were calibrated to a reversible hydrogen electrode (RHE) by using the Nernst equation:

$$E\ (RHE) = E\ (Hg/HgO) + (0.098 + 0.059\ pH)\ V \qquad \text{Equation (1)}$$

Laviron equation:

$$E_p = E_{1/2} - \left(\frac{RT}{\alpha nF}\right) \times \ln\left(\frac{\alpha nF}{RTk_s}\right) - \left(\frac{RT}{\alpha nF}\right) c \times ln(\vartheta) \qquad \text{Equation (1)}$$

E_p is the reduction potential of metal redox, $E_{1/2}$ is the formal potential of metal redox, R is universal gas constant, T is temperature in Kelvin, n is number of electrons transferred, F is the Faraday constant, α is the transfer coefficient, ks is the rate constant of metal redox, and υ is scan rate in the CV measurement. The ks and α values can be obtained from the intercept and slope of the linear graph of E_c against ln (υ).

Faraday efficiency calculation

The Faraday efficiencies of the S,V-Ni_2P/NF during the HER/OER were calculated based on the ratio of the volume of actual (V_{actual}) H_2/O_2 evolved to the theoretical one ($V_{theoretical}$):

$$\text{Faraday efficiency} = \frac{V_{actual}}{V_{theoretical}} \times 100\%$$

The actual volumes of generated H_2/O_2 gas was gathered using the drainage method. The theoretical volume can be calculated using the formula:

$$V_{\text{theoretical}} = \frac{I \cdot t \cdot V_m}{z \cdot F}$$

where I is current (A), t is time (s), V_m is molar volume of H_2/O_2 gas (28.004 L mol^{-1}, 303.15 K, 90 kPa in Urumqi, Xinjiang), F is the Faraday constant (96485 C mol^{-1}), z is electron number transferred per molecule (z is 2 and 4 for HER and OER, respectively).

Calculation method

All calculations were carried out using spin-polarized and periodic DFT implemented in the Vienna Ab initio Simulation Package (VASP) code[1]. The exchange-correlation potential was treated by using a generalized gradient approximation (GGA) with the Perdew-Burke-Ernzerhof (PBE) parametrization[2]. The van der Waals correction of Grimme's DFT-D3 model was also adopted[3]. Meanwhile, a vacuum region of about 15 Å was applied to avoid the interaction between adjacent images. The energy cutoff was set to be 450 eV. The Brillouin-zone integration was sampled with a Γ-centered Monkhorst-Pack mesh[4] of 3 × 3 × 1. The structures were fully relaxed until the maximum force on each atom was less than 0.02 eV/Å, and the energy convergent standard was 10^{-5} eV. The different charge density can be defined as $\Delta\rho = \rho_{surface} - \rho_{atoms} - \rho_{slab}$, where $\rho_{surface}$, ρ_{atoms}, and ρ_{slab} are the electron densities of the Ni_2P and S,V-Ni_2P, the isolated Ni and P (V and S)atoms, and except for the rest of the surface behind the Ni and P (V and S)atoms, respectively. The Adsorption energy (ΔE) is defined as, $\Delta E = E_{*H} - E_{*} - E_H$, where E_{*H} is the energy adsorbed by the *H on the surface, E_{*} is the energy of the surface, and E_H is the energy of the H atom under vacuum. The Gibbs free energy change (ΔG) for each elementary steps of proton-coupled electron ($H^+ + e^-$) transfer (PCET) was calculated , which has proved to be the valid first-principles computational electrochemistry technique: $\Delta G = \Delta E + \Delta E_{ZPE} - T\Delta S + \Delta G_{pH}$, where ΔE, ΔE_{ZPE}, and ΔS are the electronic energy, zero-point energy, and entropy change obtained from DFT calculations, T is the temperature (T =298.15 K), $\Delta G_{pH} = k_B T \ln 10 \times pH$(pH=14 in this work) corresponding to the correction of free energy due to the variation in H^+

concentration.

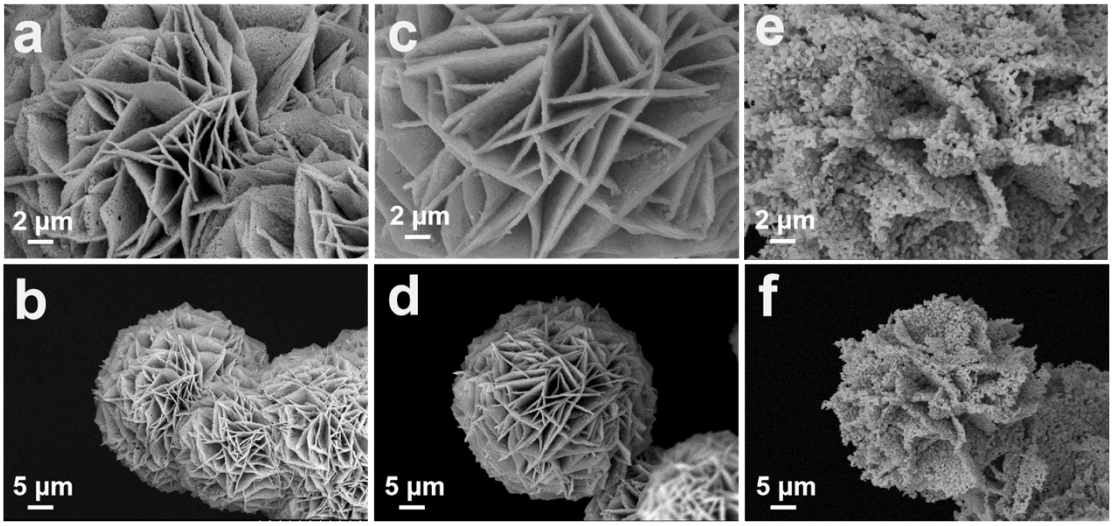

Figure S1. SEM images of (a, b) S, V-Ni_2P/NF; (c, d) V-Ni_2P/NF; (e, f) S-Ni_2P/NF.

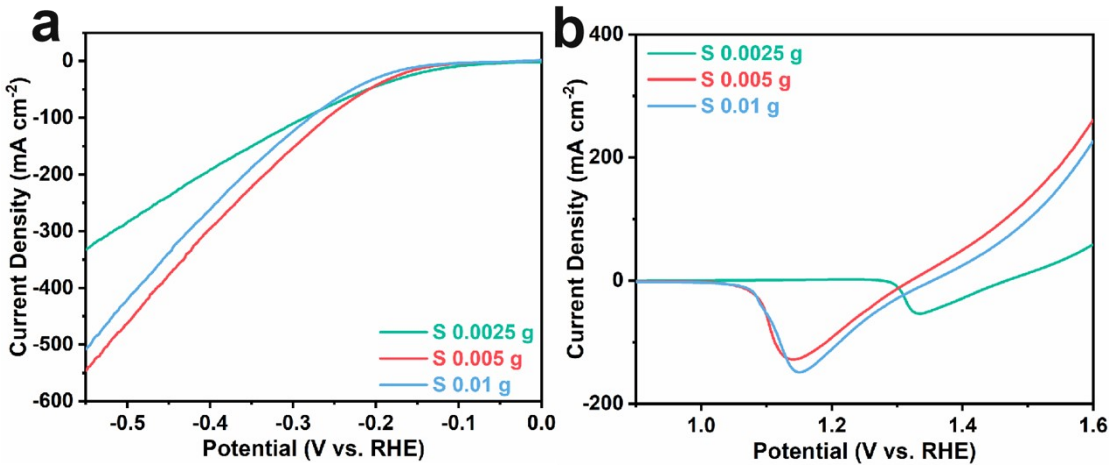

Figure S2. LSV curves of S,V-Ni_2P/NF with different S contents (a) HER; (b) OER.

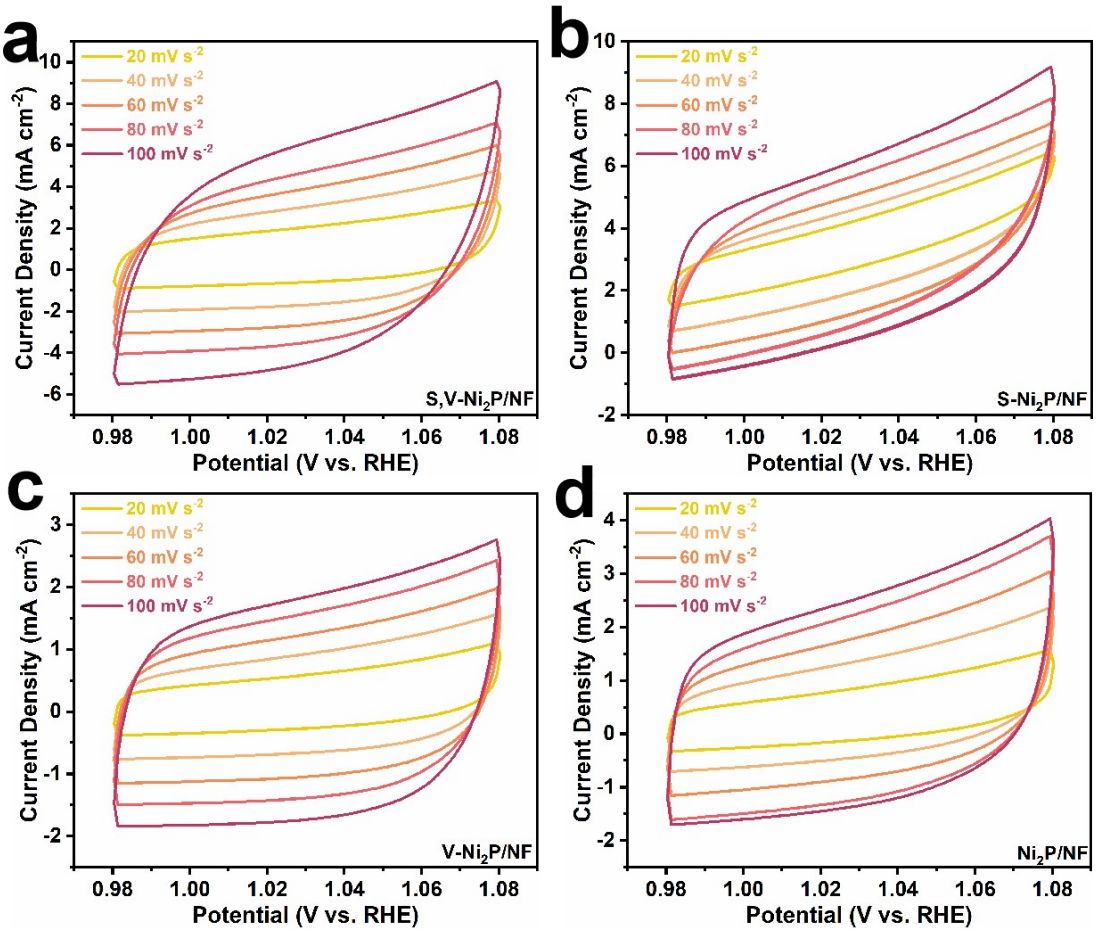

Figure S3. CV curves of (a) S, V-Ni_2P/NF, (b) S-Ni_2P/NF, (c) V-Ni_2P/NF, (d) Ni_2P/NF at different scan rates for OER.

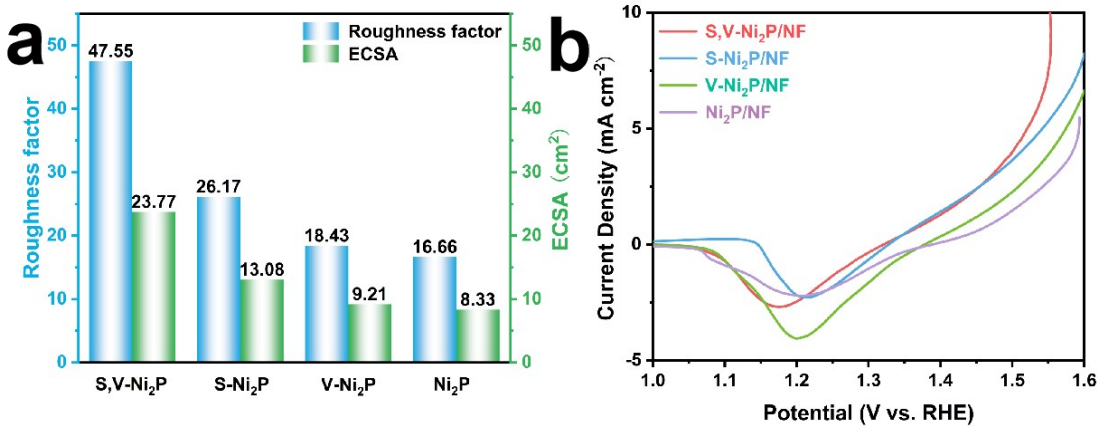

Figure S4. OER performance of samples: (a) the roughness factor (RF) and (b) the normalized polarization curve of ECSA.

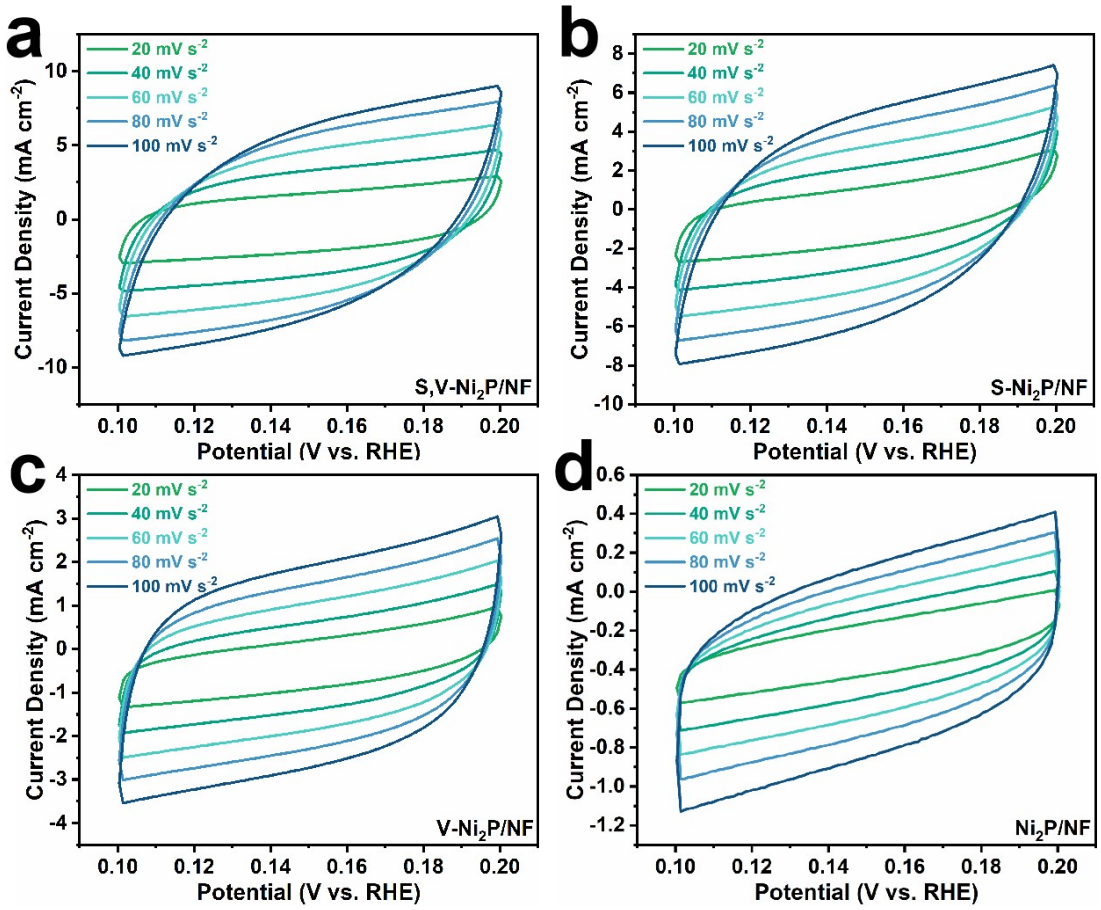

Figure S5. CV curves of (a) S, V-Ni_2P/NF, (b) S-Ni_2P/NF, (c) V-Ni_2P/NF, (d) Ni_2P/NF at different scan rates for HER.

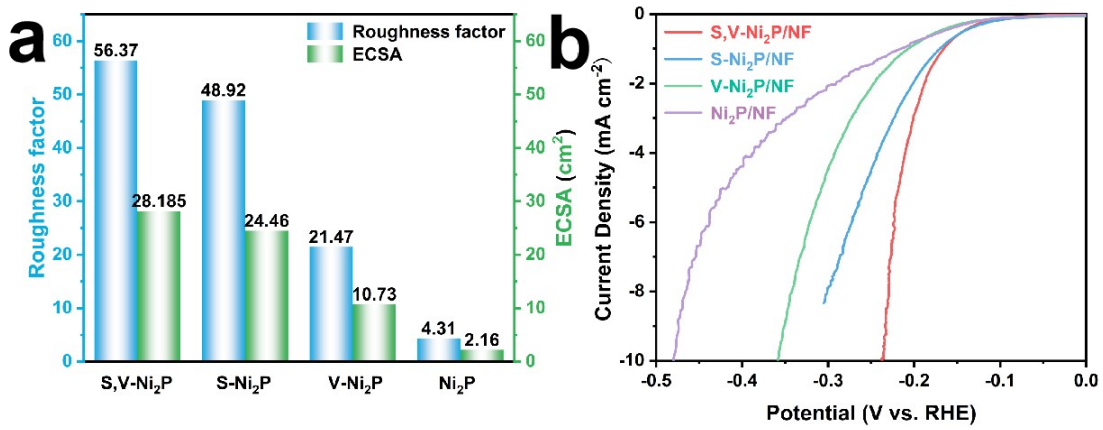

Figure S6. HER performance of samples: (a) the roughness factor (RF) and (b) the normalized polarization curve of ECSA.

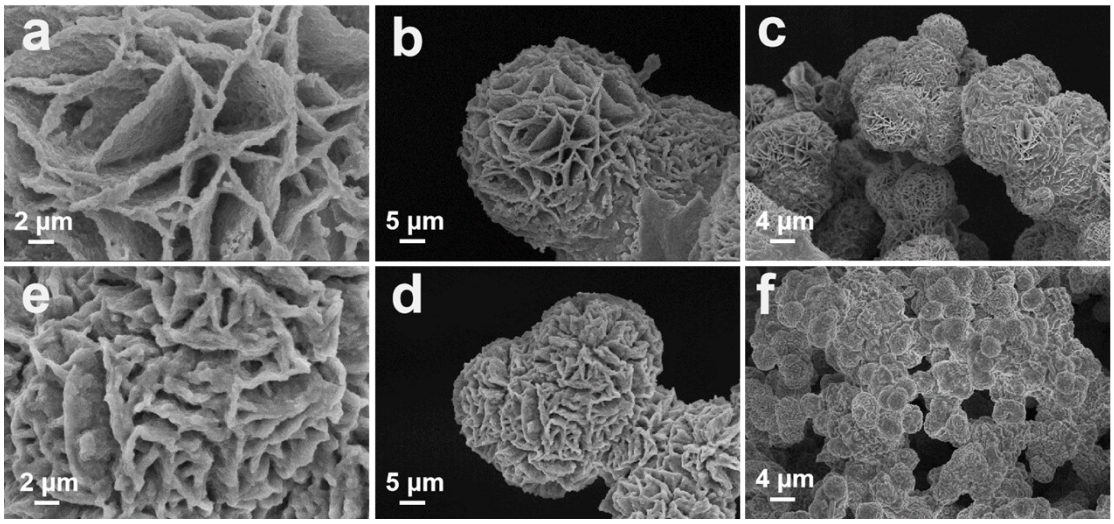

Figure S7. SEM images of the S, V-Ni_2P/NF (a-c) after OER 5000 cycles test and (e-f) after HER 5000 cycles test

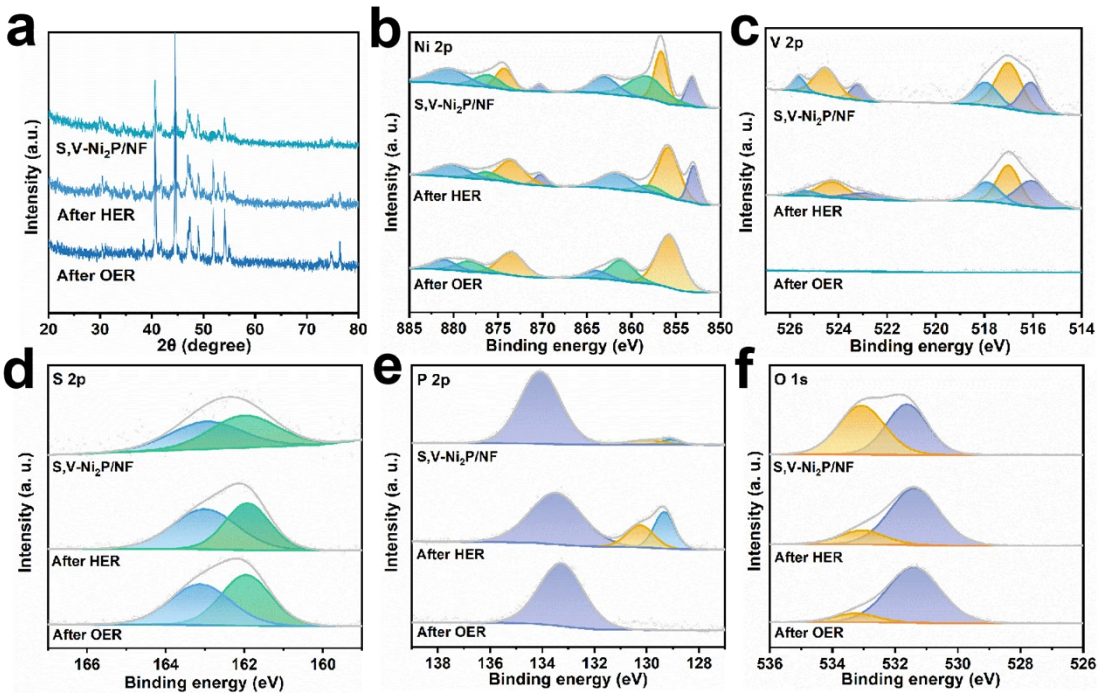

Figure S8. XRD patterns (a) and XPS spectra (b) of initial, after HER and OER test of S,V-Ni_2P/NF in 1 M KOH.

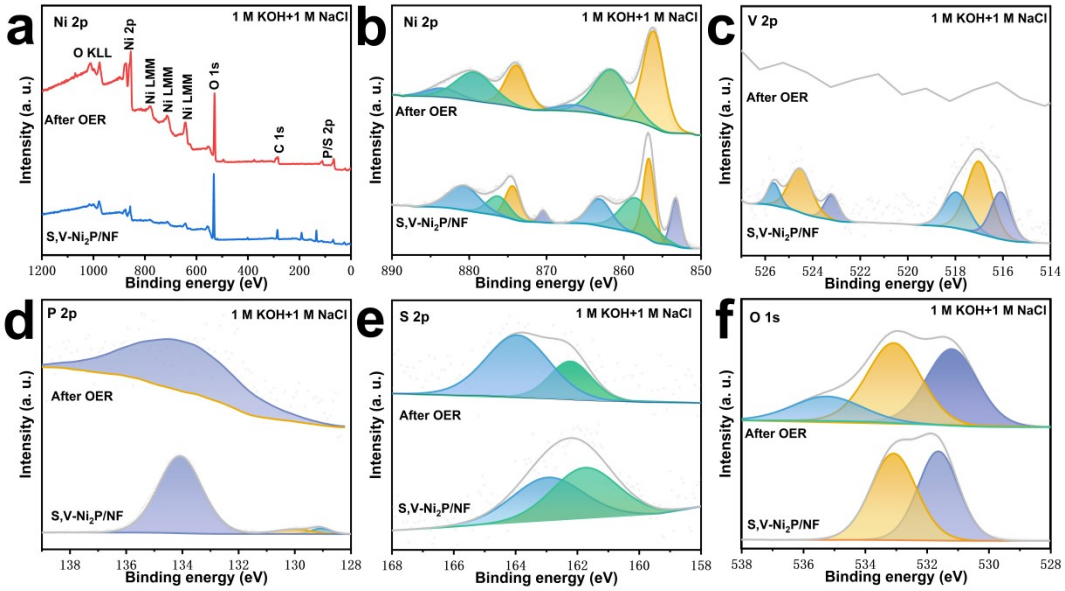

Figure S9. XRD patterns (a) and XPS spectra (b) of initial and after OER test of S,V-Ni_2P/NF in 1 M KOH+ 1 M NaCl.

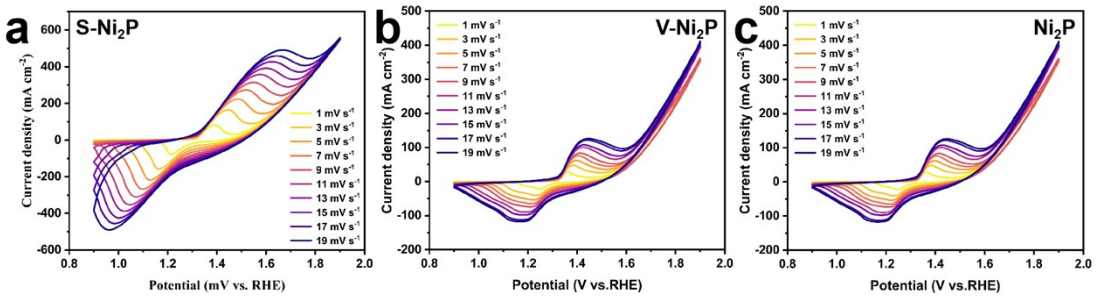

Figure S10. CV test at different scan rates for S-Ni_2P/NF (a); V-Ni_2P/NF (b); Ni_2P/NF (c).

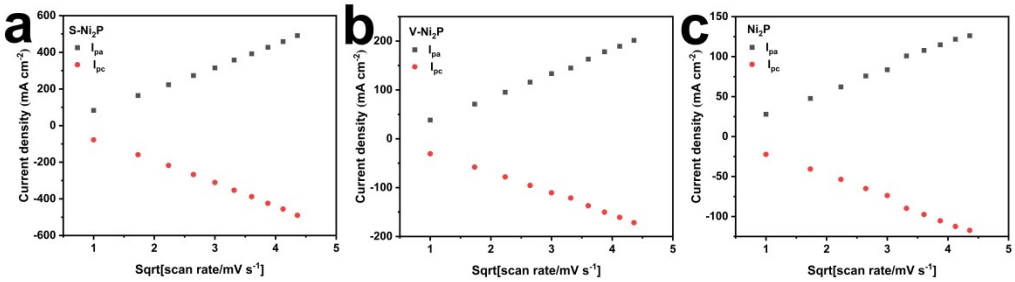

Figure S11. The obtained Ks values of S-Ni_2P/NF (a); V-Ni_2P/NF (b); Ni_2P/NF (c).

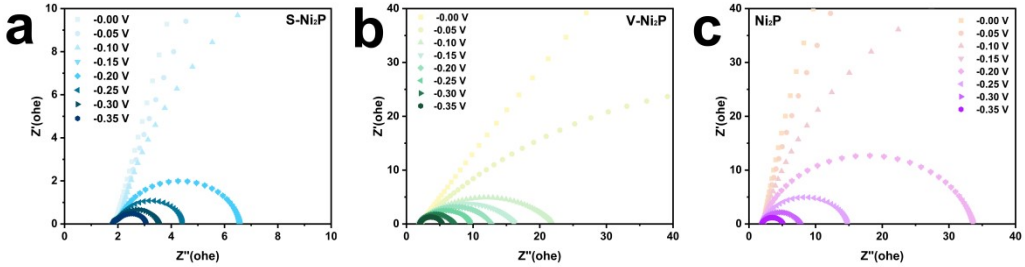

Figure S12. Nyquist plots at different potentials for S-Ni_2P/NF (a); V-Ni_2P/NF (b); Ni_2P/NF (c).

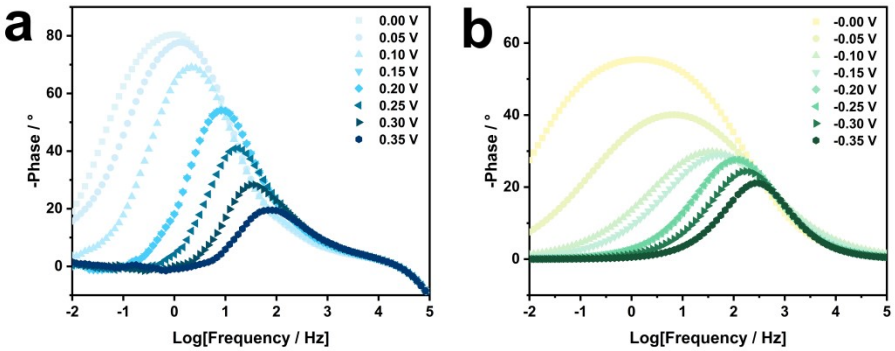

Figure S13. Bode plot at different potentials for S-Ni_2P/NF (a); V-Ni_2P/NF (b).

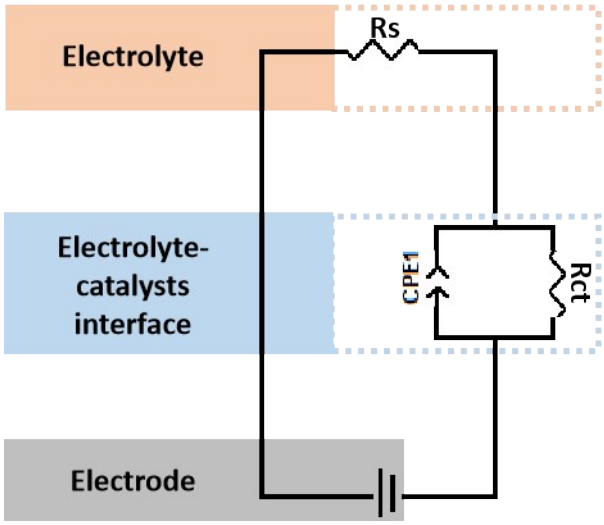

Figure S14. Equivalent circuit diagram of V-Ni_2P/NF and Ni_2P/NF.

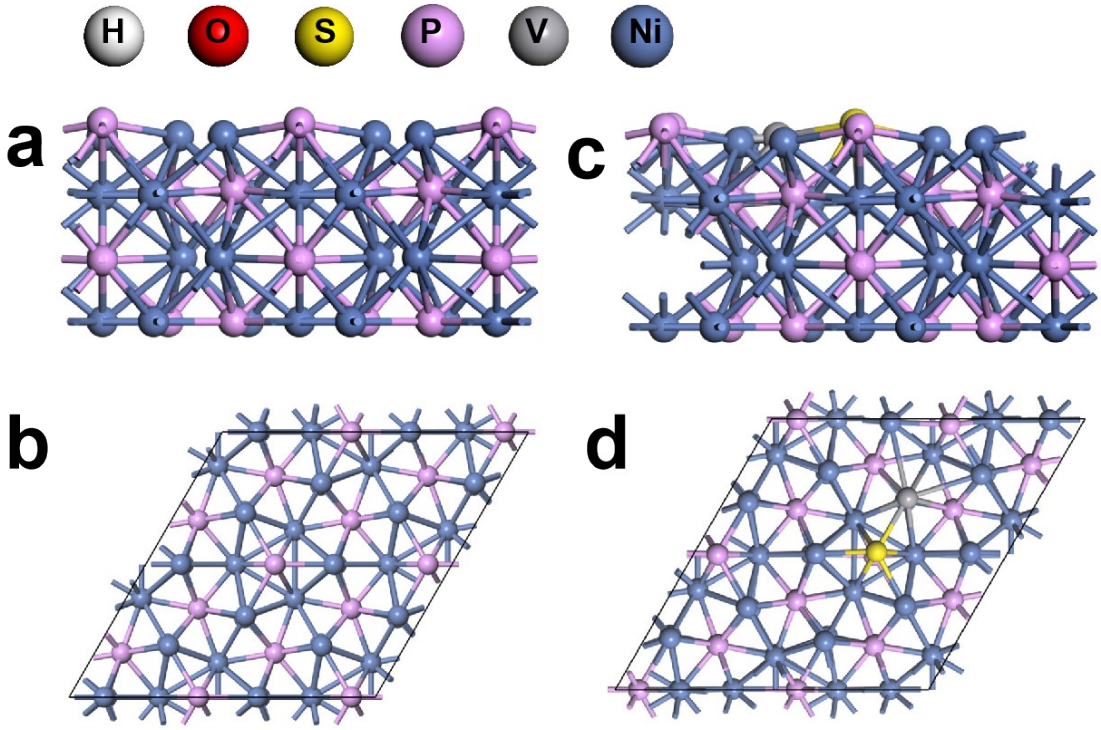

Figure S15. The structure models of Ni_2P/NF(a,b) and S,V-Ni_2P/NF (c,d).

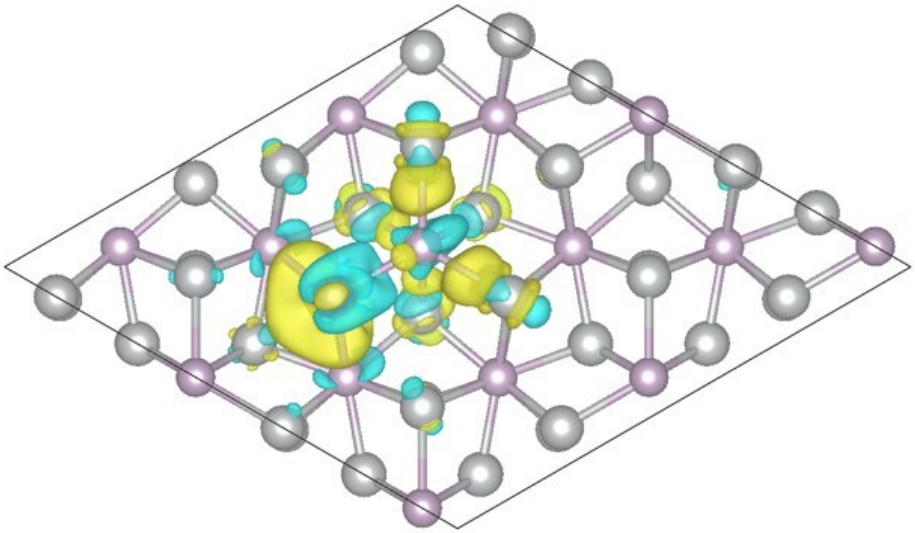

Figure S16. Differential charge diagram of Ni_2P/NF.

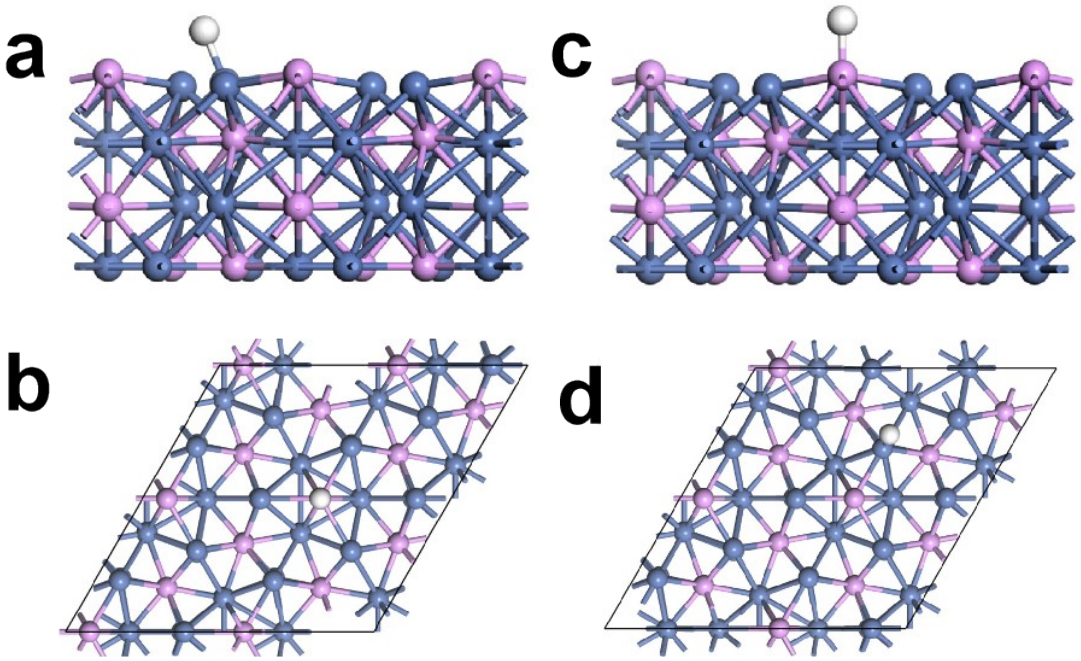

Figure S17. The H* adsorption models at Ni site (a,b) and P site (c,d) on Ni_2P/NF.

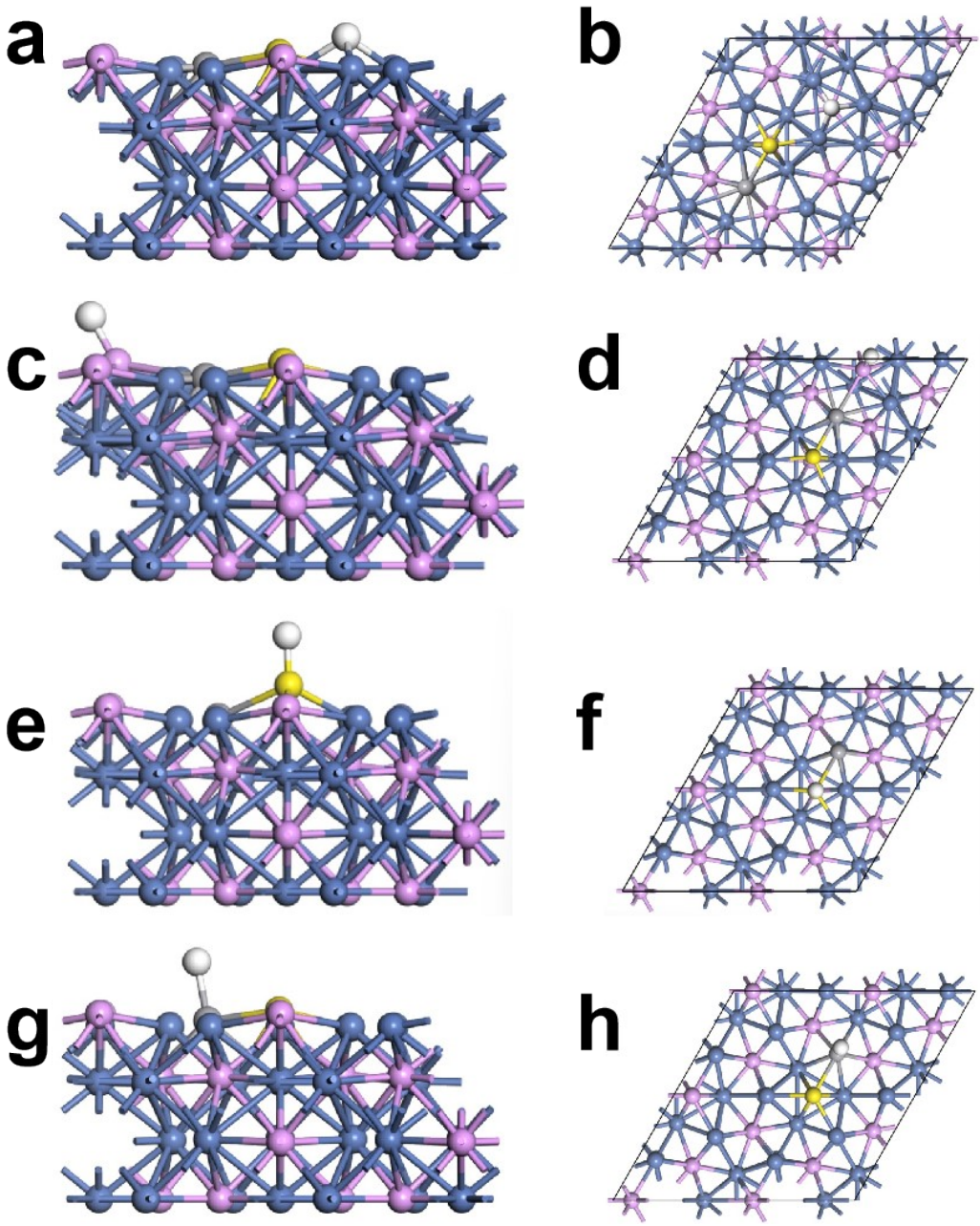

Figure S18. The H* adsorption models at Ni site (a,b), P site (c,d), V site (e,f) and S site (g,h) on S,V-Ni_2P/NF.

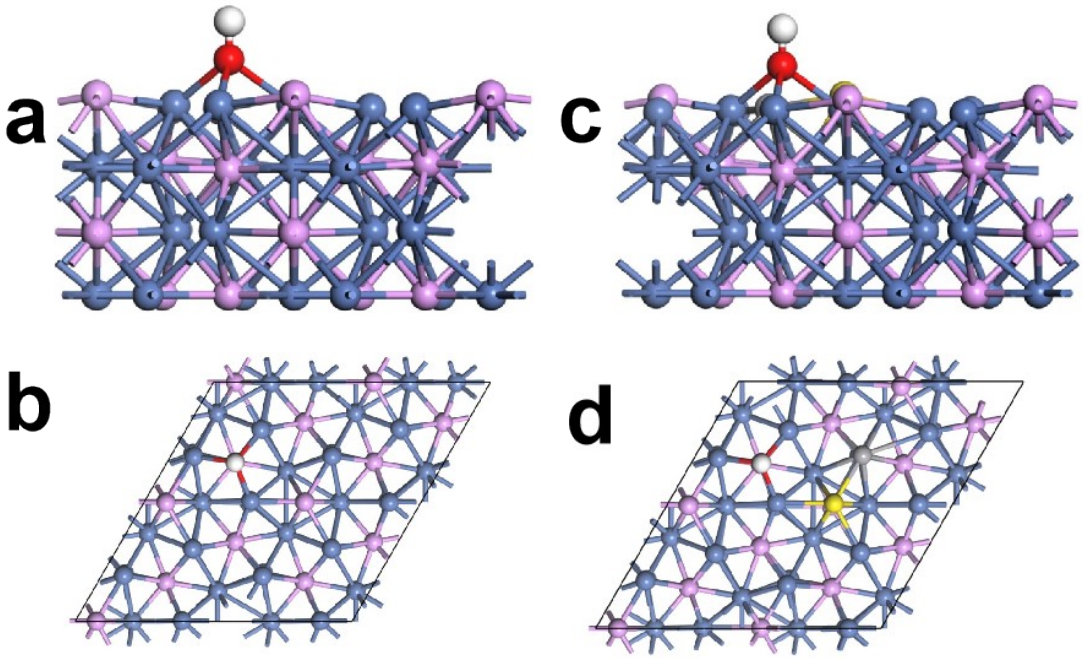

Figure S19. The OH* adsorption models at on Ni_2P/NF (a,b) and S,V-Ni_2P/NF (c,d).

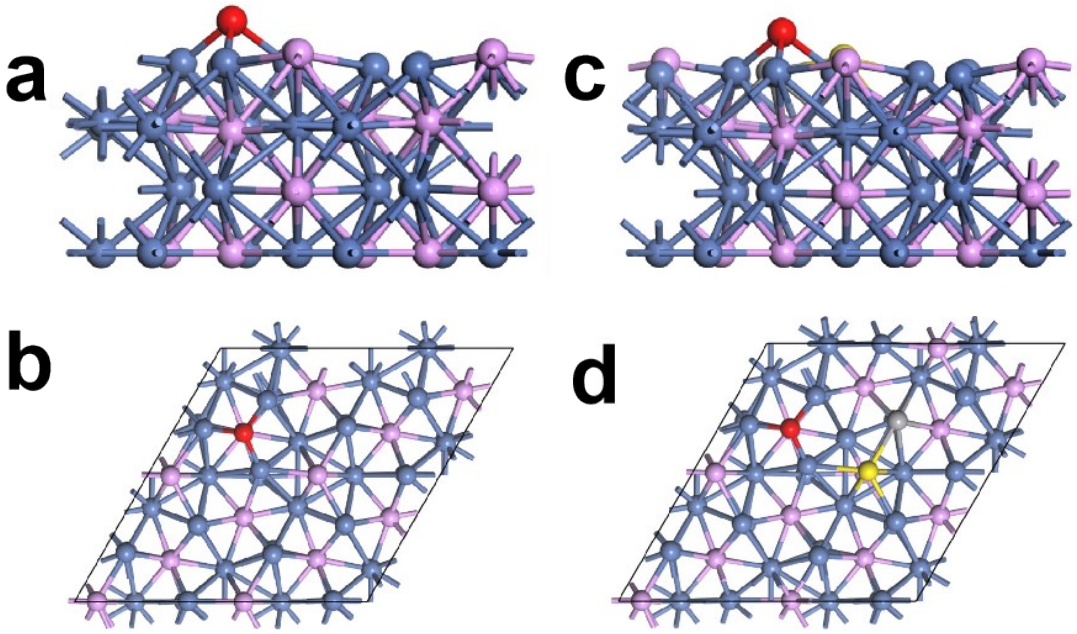

Figure S20. The O* adsorption models at on Ni_2P/NF (a,b) and S,V-Ni_2P/NF (c,d).

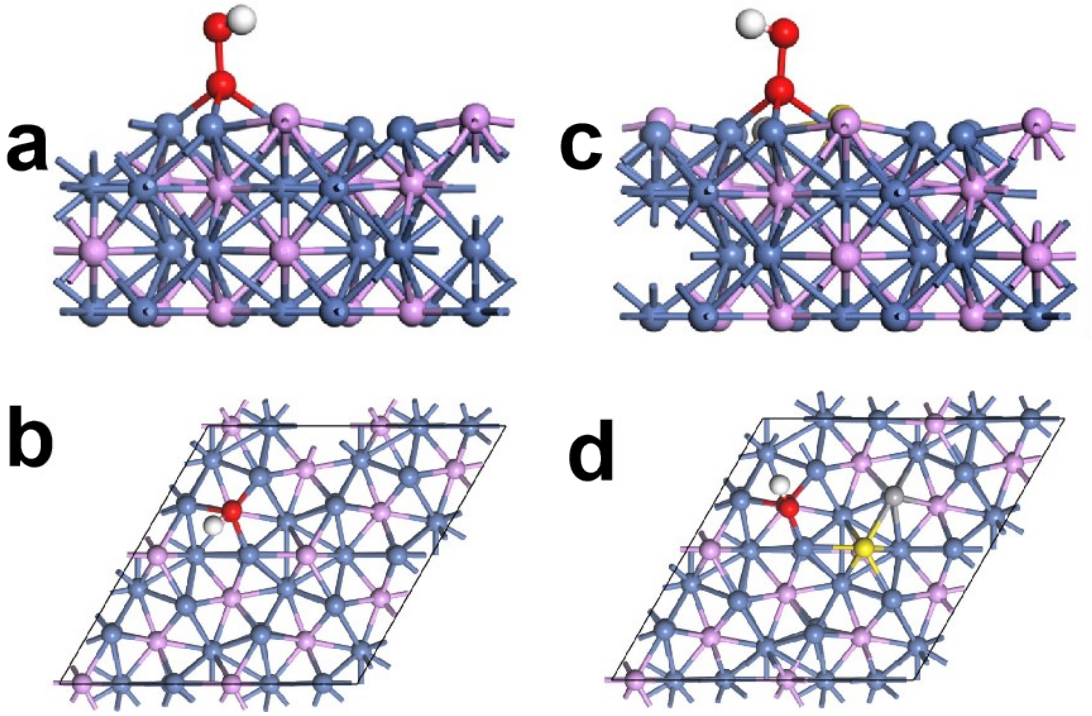

Figure S21. The OOH* adsorption models at on Ni_2P/NF (a,b) and S,V-Ni_2P/NF (c,d).

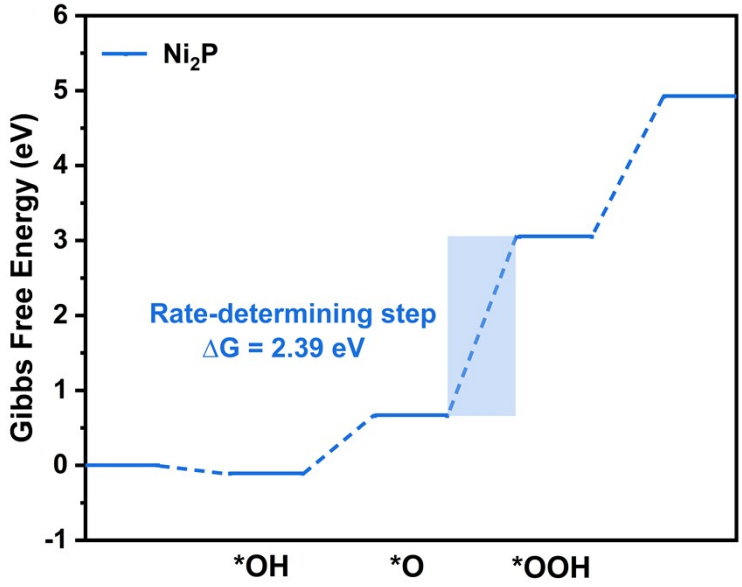

Figure S22. The free-energy diagram for the OER (f) of Ni_2P/NF.

Table S1. Energy dispersive X-ray spectroscopy data of S,V-Ni_2P/NF

Element	**Wt%**
C	8.22
O	7.95
P	23.44
S	0.26
V	0.41
Ni	59.72

Table S2. Comparison of OER of S,V-Ni_2P/NF with other reported Transition metal phosphides electrocatalys in 1 M KOH

Catalysts (Cathode)	J (mA cm^{-2})	Overpotential (mV)	Tafel slope (mV $decc^{-1}$)	Stability (h)	Reference
S,V-Ni2P/NF	100	208	30.9	200	This Work
Ni_2P/Ni foam	100	316	75	24	[1]
$Zn_{0.1}$-CoP	10	290	56	-	[2]
V-$FeNi_2P$/NF	10	200	74	48	[3]
Mo-NiCoP	100	261	58	24	[4]
NFF(V, Na)-P	100	303	52.8	180	[5]
Ni_2P-CoCH/CFP	100	320	76	50	[6]
Mo-Ni_3S_2/NixPy/NF	100	270	60.6	40	[7]
Fe,Rh-Ni_2P/NF	30	228	52.7	24	[8]
NiFeOP	10	217	62.7	40	[9]
Ni_2P-Fe_2P/NF	100	261	58	24	[10]

Table S3. Comparison of HER of S,V-Ni_2P/NF with other reported Transition metal phosphides electrocatalys in 1 M KOH

Catalysts (Cathode)	J (mA cm^{-2})	Overpotential (mV)	Tafel slope (mV $decc^{-1}$)	Stability (h)	Reference
S,V-Ni2P/NF	100	185	91.2	200	This Work
Ni_2P/Ni foam	100	222	68	24	[1]
$Zn_{0.1}$-CoP	10	98	44	-	[2]
V-FeNi_2P/NF	100	222	53	48	[3]
Mo-NiCoP	100	225	86	48	[4]
NFF(V, Na)-P	10	117	42.6	120	[5]
Ni_2P-CoCH/CFP	100	143	36	50	[6]
Mo-Ni_3S_2/NixPy/NF	10	109	68.4	24	[7]
Fe,Rh-Ni_2P/NF	10	73	117.3	24	[8]
NiFeOP	10	153	105.3	40	[9]
Ni_2P-Fe_2P/NF	100	261	58	24	[10]

Table S4. Comparison of overall water splitting activities of S,V-Ni_2P/NF with other reported Ni-based electrocatalys in 1 M KOH

Catalysts (Cathode)	Catalysts (anode)	J (mA cm^{-2})	Potential (V)	Reference
S,V-Ni2P	S,V-Ni2P	10	1.42	This Work
Ni_2P/Ni foam	Ni_2P/Ni foam	10	1.63	[1]
$Zn_{0.1}$-CoP	$Zn_{0.1}$-CoP	10	1.57	[2]
V-$FeNi_2P$/NF	V-$FeNi_2P$/NF	10	1.57	[3]
Mo-NiCoP	Mo-NiCoP	10	1.61	[4]
NFF(V, Na)-P	NFF(V, Na)-P	10	1.56	[5]
Ni_2P-CoCH/CFP	Ni_2P-CoCH/CFP	10	1.53	[6]
Mo-Ni_3S_2/NixPy/NF	Mo-Ni_3S_2/Ni_xP_y/NF	10	1.46	[7]
Fe,Rh-Ni_2P/NF	Fe,Rh-Ni_2P/NF	10	1.62	[8]
NiFeOP	NiFeOP	10	1.57	[9]
Ni_2P-Fe_2P/NF	Ni_2P-Fe_2P/NF	10	1.561	[10]
NiFeP/CC	NiFeP/CC	10	1.57	[11]
NiCoP/rGO	NiCoP/rGO	10	1.59	[12]
CoFeP/rGO	CoFeP/rGO	10	1.58	[13]
Fe_x-NiCoP/CC	Fe_x-NiCoP/CC	10	1.61	[14]
$Ni_{0.96}Co_{0.04}P$	$Ni_{0.96}Co_{0.04}P$	10	1.45	[15]

Table S5. Comparison of overall water splitting activities of S,V-Ni_2P/NF with other reported Ni-based electrocatalys in 1.0 M KOH+0.5 M NaCl

Catalysts	Electrolyte	J (mA cm^{-2})	Potential(V)	Reference
S,V-Ni2P	1.0 M KOH+ 0.5 M NaCl	10	1.48	This Work
NFF(V, Na)-P	1.0 M KOH+ 0.5 M NaCl	10	1.58	[5]
FMCO/NF	1.0 M KOH+ 0.5 M NaCl	10	1.58	[16]
Co-Ni-S/NF	1.0 M KOH+ 0.5 M NaCl	10	1.67	[17]
CoSe/$MoSe_2$	1.0 M KOH+ 0.5 M NaCl	10	1.69	[18]
NiNS	1.0 M KOH+ 0.5 M NaCl	10	1.8	[19]
NiCoP	1.0 M KOH+ 0.5 M NaCl	10	1.82	[20]
PBA/NF-2h	1.0 M KOH+ 0.5 M NaCl	10	1.83	[21]
NiCoHPi@Ni_3N/NF	1.0 M KOH+ 0.5 M NaCl	10	1.86	[22]
Mo-CoP_x/NF	1.0 M KOH+ 0.5 M NaCl	10	1.95	[23]
$CoNi_2S_4$/CC	1.0 M KOH+ 0.5 M NaCl	10	2.04	[24]

Table S6. Fitting results of S,V-Ni_2P/NF electrodes impedance spectra

S,V-Ni_2P/NF	Rs	CPE1-T	CPE1-P	Rct	CPE2-T	CPE2-P	Rmt
0.9	1.872	0.035	0.794	0.300	0.034	0.927	275.2
0.95	1.820	0.005	0.936	0.201	0.017	0.872	151.9
1.00	1.819	0.009	0.877	0.237	0.016	0.891	41.11
1.05	1.818	0.013	0.82	0.293	0.014	0.920	4.458
1.10	1.181	0.013	0.820	0.293	0.014	0.920	4.458
1.15	1.802	0.009	854	0.269	0.013	0.931	3.373
1.20	1.804	0.004	0.94	0.185	0.014	0.896	1.541
1.25	1.805	0.004	0.94	0.198	0.013	0.919	0.059

Table S7. Fitting results of S-Ni_2P/NF electrodes impedance spectra

S-Ni_2P/NF	Rs	CPE1-T	CPE1-P	Rct	CPE2-T	CPE2-P	Rmt
0.9	1.882	0.00183	1.029	0.11087	0.034542	0.8079	401.8
0.95	1.885	0.0011627	1.081	0.097881	0.03406	0.81668	141.5
1.00	1.894	0.012469	0.81638	0.19556	0.028678	0.88275	22.97
1.05	1.904	0.012666	0.81632	0.20277	0.02725	0.89981	6.83
1.10	1.914	0.015221	0.8052	0.19112	0.028263	0.89795	3.038
1.15	1.915	0.0073608	0.87311	0.16205	0.029343	0.88849	1.717
1.20	1.912	0.0029722	0.97534	0.12498	0.029809	0.86189	1.16
1.25	1.912	0.0058063	0.8986	0.16629	0.025465	0.92252	0.80488

Table S8. Fitting results of V-Ni_2P/NF electrodes impedance spectra

V-Ni_2P	Rs	CPE1-T	CPE1-P	Rct
0.9	2.086	0.0048413	0.66215	1126
0.95	1.874	0.0085788	0.56331	109
1.00	1.842	0.0076139	0.5718	20.35
1.05	1.854	0.005965	0.60946	14.48
1.10	1.912	0.0037152	0.67509	10.86
1.15	1.953	0.0023914	0.73048	7.739
1.20	1.96	0.0016651	0.76894	5.2
1.25	1.969	0.0010008	0.82593	3.409

Table S9. Fitting results of Ni_2P/NF electrodes impedance spectra

Ni_2P	Rs	CPE1-T	CPE1-P	Rct
0.9	2.129	0.00446	0.9085	952.7
0.95	2.123	0.0046	0.9081	953.1
1.00	2.082	0.005	0.869	134.2
1.05	2.019	0.003	0.862	31.37
1.10	2.022	0.003	0.861	31.43
1.15	1.986	0.003	0.831	13.02
1.20	1.941	0.003	0.8096	5.904
1.25	1.902	0.0025	0.799	3.252

[1] Y. Wu, H. Wang, S. Ji, B. G. Pollet, X. Wang, R. Wang, Nano Res. 2020, 13, 2098-2105.

[2] J. Wang, W. Li, X. Chen, A. Huang, J. Alloys Compd. 2023, 934, 167828.

[3] N. Suo, C. Chen, X. Han, X. He, Z. Dou, Z. Lin, L. Cui, J. Xiang, ACS Appl. Energy Mater. 2020, 3, 9449-9458.

[4] J. Lin, Y. Yan, C. Li, X. Si, H. Wang, J. Qi, J. Cao, Z. Zhong, W. Fei, J. Feng, Nanomicro Lett. 2019, 11, 55.

[5] Y. X. Li, J. H. Jiang, Q. H. Wu, Y. Y. Feng, Z. X. Chen, G. C. Xu, L. Zhang, Vanadium-Doped Heterogeneous Bimetallic Phosphides Derived from Layered Double Hydroxides for Saline Water Splitting, Small, 2024, 20,2402250.

[6] Shucong Zhang, Chunhui Tan, Ruipeng Yan, Xifei Zou, Fei-Long Hu, Yan Mi,*Cheng Yan,* and Shenlong Zhao*, Constructing Built-in Electric Field in Heterogeneous Nanowire Arrays for Efficient Overall Water Electrolysis, Angew. Chem. Int. Ed. 2023, 62, e202302795;

[7] Xu Luo, Pengxia Ji, Pengyan Wang, Ruilin Cheng, Ding Chen, Can Lin, Jianan Zhang, Jianwei He, Zuhao Shi, Neng Li, Shengqiang Xiao, Shichun Mu, Interface Engineering of Hierarchical Branched Mo-Doped Ni3S2/NixPy Hollow Heterostructure Nanorods for Efficient Overall Water Splitting, Advanced Energy Materials, 2020,10,1903891.

[8] Meng-Ting Chen,1 Jiao-Jiao Duan,1 Jiu-Ju Feng, Li-Ping Mei, Yang Jiao, Lu Zhang, Ai-Jun Wang, Iron, rhodium-codoped Ni2P nanosheets arrays supported on nickel foam as an efficient bifunctional electrocatalyst for overall water splitting, Journal of Colloid and Interface Science 605 (2022) 888–896.

[9] Yiming Xie, Bo Zhao, Kai Tang, Wei Qin, Changhui Tan, Junjie Yao, Youyong Li, Lin Jiang, Xianfu Wang, Yinghui Sun, In-situ phase transition induced nanoheterostructure for overall water splitting, Chemical Engineering Journal, 409, (2021), 128156.

[10] Libo Wu, Luo Yu, Fanghao Zhang, Brian McElhenny, Dan Luo, Alamgir

Karim,Shuo Chen,* and Zhifeng Ren, Heterogeneous Bimetallic Phosphide Ni2P-Fe2P as anEfficient Bifunctional Catalyst for Water/Seawater Splitting, Adv. Funct. Mater. 2021, 31, 2006484.

[11] S. Wang, J. Cai, C. Lv, C. Hu, H. Guan, J. Wang, Y. Shi, J. Song, A. Watanabe, X. Ge, Chem. Eng. J. 2021, 420, 129972.

[12] J. Li, M. Yan, X. Zhou, Z. Q. Huang, Z. Xia, C. R. Chang, Y. Ma, Y. Qu, Adv. Funct. Mater. 2016, 26, 6785-6796.

[13] X. Cai, Q. Song, D. Jiao, H. Yu, X. Tan, R. Wang, S. Luo, Int. J. Hydrogen Energy. 2022, 47, 39499-39508.

[14] M. Guo, S. Song, S. Zhang, Y. Yan, K. Zhan, J. Yang, B. Zhao, ACS Sustain. Chem. Eng. 2020, 8, 7436-7444.

[15] Xinding Lv, Shutong Wan, Tianyou Mou, Xue Han, Yifan Zhang, Zilong Wang, and Xia Tao, Atomic-Level Surface Engineering of Nickel Phosphide Nanoarrays for Efficient Electrocatalytic Water Splitting at Large Current Density, W. Liu, W. Que, R. Yin, J. Dai, D. Zheng, J. Feng, X. Xu, F. Wu, W. Shi, X. Liu, X. Cao, *Appl. Catal. B.* **2023,** *328*, 122488.

[16] S. Gopalakrishnan, V. Saranya, G. Anandha babu, S. Harish, E. Senthil Kumar, M. Navaneethan, *J. Alloys Compd.* **2023,** *965*, 171124.

[17] J. Sun, J. Li, Z. Li, C. Li, G. Ren, Z. Zhang, X. Meng, *ACS Sustain. Chem. Eng.* **2022,** *10*, 9980-9990.

[18] Y. Zhao, B. Jin, A. Vasileff, Y. Jiao, S. Z. Qiao, *J. Mater. Chem. A.* **2019,** *7*, 8117-8121.

[19] H. Liang, A. N. Gandi, D. H. Anjum, X. Wang, U. Schwingenschlögl, H. N. Alshareef, *Nano Letters.* **2016,** *16*, 7718-7725.

[20] Y. Wang, D. Jia, W. Zhang, G. Jia, H. Xie, W. Ye, G. Zhu, P. Gao, *Chem. Commun.* **2022,** *58*, 6132-6135.

[21] H. Sun, J. Sun, Y. Song, Y. Zhang, Y. Qiu, M. Sun, X. Tian, C. Li, Z. Lv, L. Zhang, *ACS Appl. Mater.Interfaces.* **2022,** *14*, 22061-22070.

[22] Y. Yu, J. Li, J. Luo, Z. Kang, C. Jia, Z. Liu, W. Huang, Q. Chen, P. Deng, Y. Shen, X. Tian, *Mater. Today Nano.* **2022,** *18*, 100216.

[23] X. Su, X. Shao, Y. Wang, W. Fan, C. Song, D. Wang, *ACS Appl. Nano Mater.* **2023**, *24*, 23029-23036.